Lab on a Chip

PAPER

View Article Online
View Journal | View Issue

Cite this: *Lab Chip*, 2020, **20**, 1648

Hybrid paper and 3D-printed microfluidic device for electrochemical detection of Ag nanoparticle labels†

Charuksha Walgama, [a] Michael P. Nguyen,[a] Lisa M. Boatner, [a] Ian Richards[b] and Richard M. Crooks *[a]

Received 17th March 2020,
Accepted 22nd March 2020

DOI: 10.1039/d0lc00276c

rsc.li/loc

In the present article we report a new hybrid microfluidic device (*hy*Flow) comprising a disposable paper electrode and a three-dimensional (3D) printed plastic chip for the electrochemical detection of a magnetic bead–silver nanoparticle (MB–AgNP) bioconjugate. This hybrid device evolved due to the difficulty of incorporating micron-scale MBs into paper-only fluidic devices. Specifically, paper fluidic devices can entrap MB-containing conjugates within their cellulose or nitrocellulose fiber matrix. The *hy*Flow system was designed to minimize such issues and transport MB conjugates more efficiently to the electrochemical detection zone of the device. The *hy*Flow system retains the benefit of fluid transport by pressure-driven flow, however, no pump is required for its operation. The *hy*Flow device is capable of detecting either pre-formed MB–AgNP conjugates or conjugates formed *in situ*. The detection limit of AgNPs using this device is 12 pM, which represents just 22 AgNPs per MB.

Introduction

Herein we report a hybrid microfluidic device (*hy*Flow) composed of a paper electrode and a three-dimensional (3D) printed plastic chip intended for electrochemical detection of bioconjugated silver nanoparticle (AgNP) labels. The key finding is that the *hy*Flow device is capable of detecting preformed magnetic bead–AgNP (MB–AgNP) conjugates at AgNP concentrations as low as 12 pM. Additionally, we show that these conjugates can be formed *in situ* within the flow channel from separate, dried-down components. The device is shown in Scheme 1. Scheme 1a represents the wax printed paper electrode platform, which incorporates the screen-printed carbon electrodes. This paper electrode was designed to slide into an edge connector, which has compressible crimp terminals for providing an ohmic electrical contact. Scheme 1b is the 3D-printed microfluidic chip, which comprises two pieces. The top piece has an inlet for sample addition while the bottom piece contains a hollow microfluidic channel, an electrochemical detection zone, and an outlet reservoir.

The *hy*Flow is a significant advance for microfluidic biosensing applications for four reasons. First, it uses a disposable paper-based electrode insert to ensure low cost and to aid in reagent storage. Second, the hollow channel within the 3D-printed plastic chip facilitates transport of micron-scale particles and minimizes nonspecific adsorption. This is in contrast to traditional paper-only devices in which particles become entrapped within the cellulose fiber network.[1,2] Third, the biotin–streptavidin conjugate that links the AgNPs and MBs can be formed within the microfluidic channel in <2 min following hydration and passive diffusive mixing of the individual, dried-down assay components. Therefore, the device does not require an active, and hence complex, means of mixing. Fourth, the *hy*Flow device is capable of detecting AgNP labels at concentrations as low as 12 pM, which represents just 22 AgNPs per 1.0 μm-diameter MB.

Point-of-care (PoC) technologies are important because they are capable of providing fast (typically <10 min) diagnostic testing in non-laboratory and resource-limited environments.[3–5] Among the large variety of PoC sensing strategies, paper-based lateral flow test formats are attractive due to their low cost, portability, and simplicity.[6,7] In most cases, these devices are used to detect a single analyte: the classic case being the home pregnancy test for human chorionic gonadotropin hormone.[8] Starting in 2007, Whitesides and co-workers extended the lateral flow concept to include multidimensional geometries that could sense multiple analytes upon application of a single sample.[9,10]

[a] *Department of Chemistry and Texas Materials Institute, The University of Texas at Austin, 100 East 24th Street, Stop A1590, Austin, Texas 78712-1224, USA. E-mail: crooks@cm.utexas.edu; Tel: +512 475 8674*
[b] *Interactives Executive Excellence LLC, Austin, Texas 78733, USA*

† Electronic supplementary information (ESI) available. See DOI:10.1039/d0lc00276c

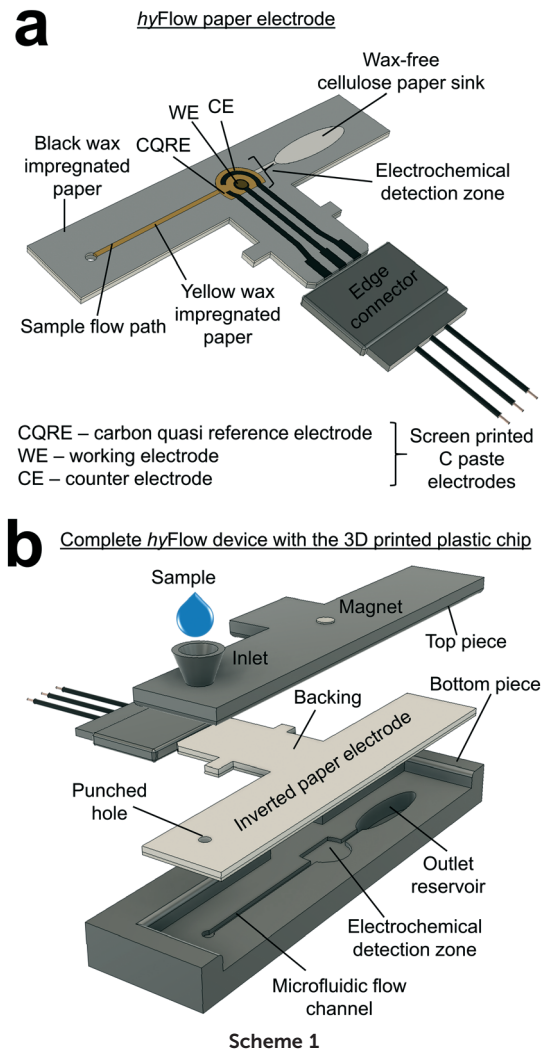

Scheme 1

Since their introduction, these microfluidic paper-based analytical devices (μPADs) have evolved to provide sophisticated and multiplexed analyses.[11–14] Our group has contributed to this evolution by introducing origami-based fabrication methods,[15,16] electrochemical detection,[17–19] and hollow channels for rapid fluid processing.[20–22]

Because they are robust and sensitive, electrochemical detection schemes have previously been incorporated into μPADs.[23,24] Electrochemical lateral flow immunosensors have also been reported for a vast range of analytes including: viral proteins,[25,26] cardiovascular disease markers,[27,28] biological warfare agents,[29] and immunologically important enzymes.[30] Our group developed an electrochemical strategy to detect AgNP-labeled bioconjugates on paper devices in 2014.[31] Specifically, we showed that AgNPs can be oxidized by either chemical means[18,19,31] or by a galvanic exchange (GE) reaction.[32–34]

Transport of micron-scale magnetic beads through paper channels is a challenge, because, as mentioned earlier, they can become trapped within a cellulose or nitrocellulose fiber matrix.[1,2,35,36] To remedy this problem, we reported on the development of hollow channel paper fluidic devices, however even in this format MB transport can be hindered.[18,31,32] Henry and coworkers have also reported a method for preparing hollow paper channels, but it suffers from the same problems.[37] We conclude that paper-only devices, as presently configured, are not reliable platforms for transport of micron-scale particles.

To address the deficiencies of paper-only microsystems, we have developed the simple hybrid paper and 3D-printed microfluidic *hy*Flow device shown in Scheme 1. The *hy*Flow is capable of carrying out four types of model assays (Scheme 2). The first of these we call a 'wet' assay. In this case, the model MB–AgNP conjugate is prepared off-chip and then the suspension is pipetted into the inlet of the device. The second is a 'dry' assay, in which the preformed MB–AgNP conjugate is dried onto the paper electrode strip and subsequently resolvated prior to analysis. We call the third type of assay 'instant mix-1'. Here, streptavidin-coated MBs predeposited and dried within the channel are resolvated using a solution containing biotin-labeled AgNPs. In other words, the conjugate is formed *in situ* starting with just one dried-down component. Finally, the fourth assay, 'instant mix-2', involves resolvation and subsequent conjugation of two components predried in separate zones on the test strip channel: streptavidin-coated MBs and biotin-labeled AgNPs.

On the basis of the foregoing four types of assays, we show that the *hy*Flow device is capable of storing, resolvating, and conjugating individual assay components of a model MB–AgNP analyte system. In contrast to the paper-only devices that have been previously reported,[18,31,38] the *hy*Flow delivers a substantial fraction of the MB–AgNP conjugates to the detection zone where they are reproducibly detected by electrochemical means. Moreover, the novel paper and 3D-printed hybrid design of the *hy*Flow device not only facilitates the incorporation of a rigid hollow channel for fluid processing, but also retains its compatibility to store reagents on the paper ceiling of the microfluidic channel to aid on-chip assay formation.

Experimental section

Chemicals and materials

All solutions were made using deionized (DI) water (>18.0 MΩ cm, Milli-Q Gradient System, Millipore, Bedford, MA). NaCl, NaOH, HCl, $HAuCl_4$, KNO_3, KCl, $K_3[Fe(CN)_6]$, citric acid monohydrate, 4-(2-hydroxyethyl)-1-piperazineethanesulfonic acid (HEPES), isopropanol, SuperBlock blocking buffer in PBS, Whatman grade 1 chromatography paper (180 μm thick, 20 cm × 20 cm sheets, linear flow rate of water = 0.43 cm min^{-1}), and siliconized low-retention microcentrifuge tubes were purchased from Fisher Scientific (Pittsburgh, PA). Boric acid was purchased from EM Science (Gibbstown, NJ). Citrate-capped AgNPs (nominal 20 nm diameter, 6.0×10^{11} AgNPs per mL) were purchased from Ted Pella (Redding, CA). Sucrose and D-(+)-trehalose dihydrate were purchased from Millipore-Sigma (Burlington, MA). A solution containing 0.10

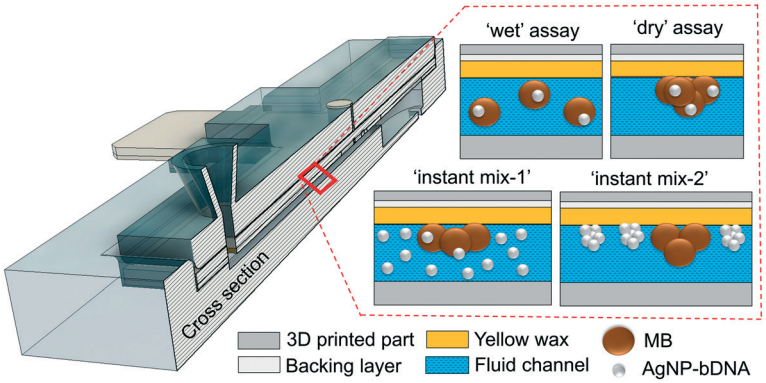

Scheme 2

M borate and 0.10 M NaCl (referred to henceforth as BCl) was prepared by dissolving appropriate amounts of boric acid and NaCl in DI water, and then adjusting the pH to 7.5 with NaOH. A separate set of BCl solutions was prepared using different mass percentages of sugar (2, 10, 20, and 50 wt%) by adding 1 : 1 mixtures of sucrose and D-(+)-trehalose dihydrate, and they will be denoted henceforth as BClS(2%), BClS(10%), BClS(20%), and BClS(50%). These borate solutions primarily serve as supporting electrolytes and storage media for MB–AgNP conjugates under different assays conditions.

Conductive carbon paste (Cl-2042) was purchased from Engineered Conductive Materials (Delaware, OH). Cylindrical neodymium magnets (0.12 inch diameter: N42P120060; 0.50 inch diameter: N42P500060) were purchased from Bunting Magnetics Co. (Newton, KS). Streptavidin-coated, 1.0 μm-diameter MBs (Dynabeads, MyOne Streptavidin T1, 10 mg mL^{-1}, ~7–10 × 10^9 MB per mL, binding capacity: 1100–1700 pmol mg^{-1} of free biotin) and 2.8 μm-diameter MBs (Dynabeads, M-270 Streptavidin, 10 mg mL^{-1}, ~6–7 × 10^8 MB per mL, binding capacity: 650–900 pmol mg^{-1} of free biotin) were obtained from Invitrogen (Grand Island, NY). Smaller size MBs were purchased from Ademtech (Pessac, France): ~227 nm diameter (Bio-Adembeads Streptavidin Plus 0322, 5 mg mL^{-1}, ~4.5 × 10^{11} MB per mL, binding capacity: 4475 pmol mg^{-1} of free biotin). Lyophilized thiol-DNA-biotin (5′d thiol C6 SSACATTAAAATTC-biotin 3′) was purchased from Biosearch Technologies (Petaluma, CA). Before use, the DNA-biotin was hydrated with the appropriate amount of DI water to yield a final concentration of 1.0 mM.[32]

A4-sized Kodak photo paper and clear acrylic spray (Krylon) were purchased from Staples, Inc. (Framingham, MA).

Fabrication of paper electrodes (*hy*Flow and *no*Flow devices)

Fig. S1† is the CAD drawing of the *hy*Flow paper electrode. These electrodes were fabricated by stencil-printing carbon paste onto wax-patterned sheets of chromatography paper (Fig. S2†). Some control experiments intended to investigate the effect of sugar on interfacial electrochemistry and GE were carried out using a simplified version of the *hy*Flow paper electrode, which is termed the *no*Flow electrode (Fig. S3†). Detailed fabrication procedures of both *hy*Flow and *no*Flow devices are provided in the ESI.†

Note that Au was electrochemically deposited onto the carbon paste working electrodes (WEs) of both the *hy*Flow and *no*Flow paper electrodes only when they were used to detect MB–AgNP conjugates. This was necessary because the MB–AgNP conjugates are detected using a GE reaction, which will be discussed in detail later, between electrogenerated Au^{3+} ions and conjugated AgNPs.

Unless otherwise indicated, Au was electrochemically deposited onto the carbon paste WE as follows. A droplet (50.0 μL) of solution containing 6.0 mM $HAuCl_4$ and 0.10 M KNO_3 was pipetted atop the electrochemical detection zone, and then a potentiostat was used to step the potential of the WE from 0 to −0.60 V (*vs.* CQRE). The duration of the potential step was 2.0 s. Some control experiments carried out using the *no*Flow device, which did not involve MB–AgNP conjugates, were performed in the absence of electrodeposited Au.

3D printing

The *hy*Flow device consists of a paper electrode and a 3D-printed chip. The chip is composed of two pieces. The top piece, or ceiling, of the chip has an inlet (Fig. S4a†) and the bottom piece, or floor, contains the microfluidic channel (Fig. S4b†). These individual parts were 3D printed using a Form 2, stereo lithography printer from Formlabs (Somerville, MA). Additional details relating to the fabrication procedure and the assembly of the *hy*Flow device (Fig. S5†) are provided in the ESI.†

Preparation of biotin-labeled AgNPs and MB–AgNP conjugates

Biotinylated DNA was immobilized onto 20 nm AgNPs using a previously reported fast, pH-assisted method.[32,34,39] This construct will henceforth be referred to as 'AgNP-bDNA'. Fig. S6† illustrates the preparation of MB–AgNP stock conjugate suspensions, samples prepared from these stock

Table 1 Characteristics of the MB–AgNP conjugates detected using the *no*Flow and *hy*Flow devices under the indicated experimental conditions

Sample type	Estimated AgNP : MB ratio	Estimated [AgNP] in the sample (pM)	Description of the experiment (see Results and discussion section for more details)	Device
Sample-0	441	125	Absence of sugar modifications	*no*Flow
Sample-1	441	125	Effect of sugar dried on the WE	*no*Flow
Sample-2	441	125	Effect of sugar dissolved in solution	*no*Flow
Sample set-3	441	249	Effect of sugar on 'wet' assay	*hy*Flow
Sample set-4	441	249	Effect of sugar on 'dry' assay	*hy*Flow
Sample set-5	22–1765	12–996	Dose–response: 'wet' assay	*hy*Flow
Sample set-6	22–1765	12–996	Dose–response: 'dry' assay	*hy*Flow

suspensions, and the application of these samples in the *hy*Flow and *no*Flow devices. All these MB–AgNP conjugate types, their concentrations and performed experiments are summarized in the Table 1. Four different types of assays ('wet', 'dry', 'instant mix-1' and 'instant mix-2') were examined using the *hy*Flow device. The specific protocols used for these experiments are discussed later.

The concentrations of MB–AgNP conjugates were calculated using the following two methods. First, assuming all added AgNP-bDNA are uniformly distributed on the MBs, the number of AgNPs bound to a single MB was estimated as the AgNP : MB ratio. The second estimate is based on the final concentration of AgNPs present in the 50.0 μL conjugate sample introduced into the device during the 'wet' assay. These estimated values are presented in Table 1 and Table S1.† Note that UV/vis spectroscopic data confirm complete attachment of AgNP-bDNA to the MBs (Fig. S7†).

Electrochemistry

All electrochemical measurements were performed using a CH Instruments electrochemical workstation (Model 120b, Austin, TX).

Contact angle measurements

Contact angles were quantified using a FTA200 Goniometer (First Ten Angstroms, Portsmouth, VA).

Scanning electron microscopy (SEM)

SEM micrographs were obtained using a Hitachi S5500 SEM instrument having an accelerating voltage of 30 kV, and a point-to-point resolution of 0.4 nm.

Results and discussion

Description and operation of the *hy*Flow device

The hybrid paper and 3D-printed *hy*Flow device used for electrochemical detection of AgNP-labeled magnetic beads (MB–AgNP) is illustrated in Scheme 1 and described in detail in the Experimental section. The paper electrode assembly (Scheme 1a) features a sample flow path, an electrochemical detection zone (printed with yellow wax, which is slightly more hydrophilic than black wax as shown in Fig. S8†), and a sink consisting of wax-free cellulose paper. Three carbon paste electrodes are screen printed in the electrochemical detection zone: the WE, the carbon quasi-reference electrode (CQRE), and the counter electrode (CE). For most experiments, Au is electrodeposited onto the WE. After fabricating the electrode assembly, the *hy*Flow device was assembled as discussed in the ESI† section.

An inlet is present in the top piece of the *hy*Flow device for sample injection (Scheme 1b and Fig. S4a†). To ensure spontaneous pressure-driven flow, the sample inlet was designed to have a height of 5.0 mm above the plane of the top piece. The bottom piece of the chip contains a microfluidic channel that is colinear with the sample flow path on the paper. It also incorporates an outlet reservoir that facilitates sample flow through the electrochemical detection zone (Fig. S4b†). The fluid flow rate within the *hy*Flow device is ~420 μL min^{-1}. As the sample flows toward the outlet reservoir, a magnet, located in the top piece of the chip, concentrates the MB–AgNP conjugate onto the WE. Electrochemical detection of the conjugate is initiated after the conjugate is immobilized on the WE.

Galvanic exchange

The GE process that takes place in both the *no*Flow and *hy*Flow devices is summarized in eqn (1), and illustrated in Fig. 1a.

$$3Ag^0_{(s)} + Au^{3+}_{(aq)} \rightarrow 3Ag^+_{(aq)} + Au^0_{(s)}\ \Delta E^\circ = 0.70\ V \quad (1)$$

Under standard conditions, the driving force for eqn (1) can be calculated from the difference in the standard potentials of the individual half reactions: ΔE° = 0.70 V.[40] Specifically, the GE reaction occurs between zero-valent AgNPs, present in the MB–AgNP conjugates, and electrogenerated Au^{3+} ions. Briefly, after concentrating the MB–AgNP conjugates onto the WE, the potential was stepped from 0 to 0.80 V (all potentials are *vs.* CQRE unless otherwise indicated) for 12.0 s. This results in oxidation of a fraction of the previously electrodeposited Au^0, which initiates the GE reaction. GE proceeds for 1.0 s, and then the electrode potential is stepped from 0 to −0.70 V for 50.0 s to electrodeposit the resulting Ag^0 onto the electrode surface. This series of steps is defined as one GE cycle. We have found, however, that two GE cycles maximizes the amount of Ag deposited onto the WE.[34] Accordingly, after two GE cycles, the amount of Ag^0

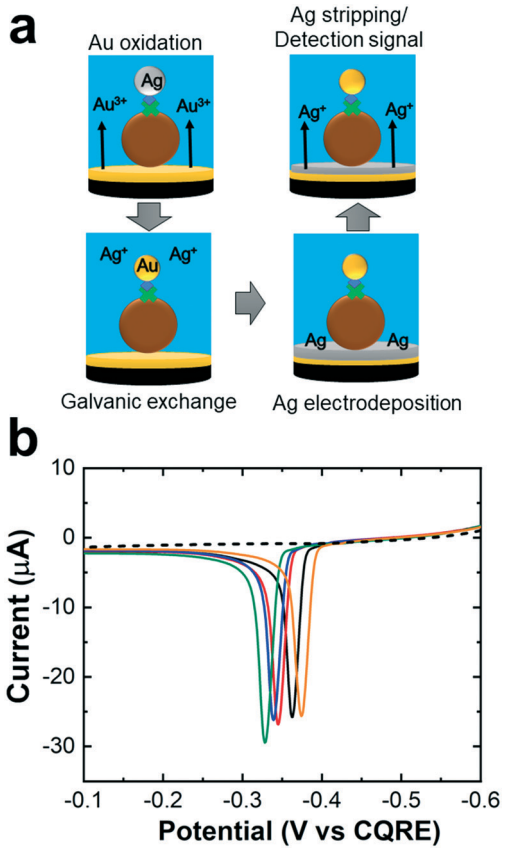

Fig. 1 (a) Schematic representation of the GE process. (b) ASVs for detection of MB–AgNP conjugate using five independently fabricated *no*Flow devices. The dashed line represents the signal collected on a *no*Flow device in the absence of electrodeposited Au. MB–AgNP conjugate: sample-0 (Table 1 and Fig. S6†); electrolyte: BCl; scan rate: 0.050 V s^{-1}; T = ~25 °C. The ASV peaks are at different potentials due to the use of a carbon QRE.

residing on the electrode is determined by anodic stripping voltammetry (ASV). That is, following two GE cycles, the WE electrode potential is scanned twice from −0.70 V to 0.20 V, and the resulting charge is calculated by integrating the charge under the peak corresponding to the second ASV.

Fig. 1b shows ASVs obtained for detection of the MB–AgNP conjugate using five independently fabricated *no*Flow devices. In these experiments the concentration of the AgNPs was 125 pM (Table 1 and Fig. S6:† sample-0). The average GE/ASV charge recovered in these experiments was 12.5 ± 0.4 μC, which reflects the reproducibility of the electrochemical detection method. The black dashed line in Fig. 1b was obtained for an identical experiment, but in the absence of electrodeposited Au on the WE. In this case, there is no detectable level of charge, indicating that the AgNPs are not in direct contact with the electrode. The different peak positions are a consequence of variability in the potential of the CQRE, but this does not affect the analysis which depends only on the charge under the peaks.

Effect of sugar on redox electrochemistry and GE

The point-of-care device format that we envision will have all necessary reagents in a dried-down state immobilized in the test device and these reagents will be rehydrated at the time of use. A mixture of sugars is often used for stabilizing dried biological reagents on lateral flow devices. There are two reasons for this. First, sugars can prevent protein degradation by creating an inert and glassy solid matrix around the protein molecules.[41] Second, sugars are capable of forming hydrogen bonding networks with proteins, which serve as a substitute for the stabilizing influence of water.[42] For example, Chen *et al.* recently reported that proteins dried in a sugar matrix composed of 10 wt% sucrose plus 10 wt% of D-(+)-trehalose and dehydrated on a paper device retained 80% of their activity after 30 days of storage at 25 °C.[43] We decided to adopt this approach but were concerned that the presence of sugar could interfere with the electrochemical processes used in the metalloimmunoassay. Accordingly, we carried out the following control experiments.

First, 10.0 μL of a BClS(20%) solution was pipetted onto the screen-printed carbon WE of a *no*Flow electrode (no electrodeposited Au) and allowed to dry for 4 h under ambient laboratory conditions (~25 °C). Second, a 50.0 μL solution containing 10 mM $K_3[Fe(CN)_6]$ and 0.10 M KCl was pipetted into the *no*Flow cell. After a few seconds, a series of cyclic voltammograms (CV) was obtained to determine the effect of dried, and subsequently resolvated, sugar on the performance of the electrochemical cell. The results are

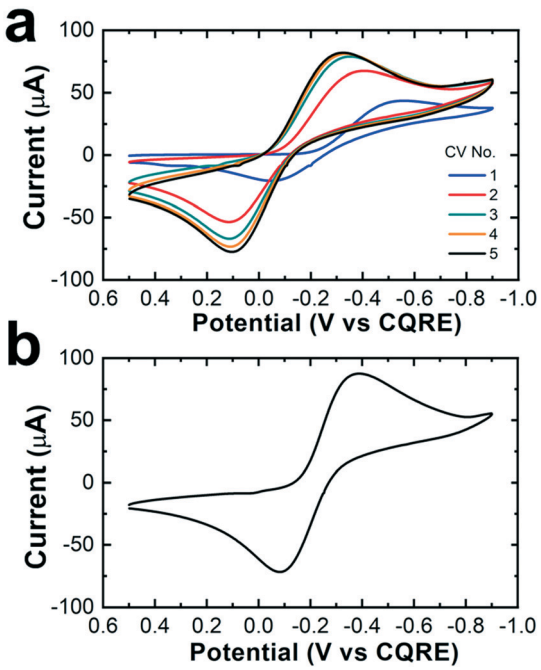

Fig. 2 CVs obtained in 10.0 mM $K_3[Fe(CN)_6]$ plus 0.10 M KCl in the (a) presence and (b) absence of sugar dried onto the *no*Flow carbon WE. For these experiments, Au was not electrodeposited onto the WE. In (a) multiple, sequential CVs are shown; the order in which they were obtained is provided in the legend. Scan rate: 0.050 V s^{-1}; T = ~25 °C.

shown in Fig. 2a. The shapes of the first two CVs indicate partial electrode passivation by sugar,[44] but by the third scan the CV attains a limiting shape with a cathodic peak current ($i_{p,c}$) = 70 ± 11 μA, $E^{\circ\prime}$ = −0.12 ± 0.01 V, and splitting between the two peaks (ΔE_p) = 0.40 ± 0.03 V.

We carried out a control experiment identical to the one described in the previous paragraph, but in the absence of sugar (10.0 mM $K_3[Fe(CN)_6]$ plus 0.10 M KCl only). The first CV for this control experiment is shown in Fig. 2b. Here, $i_{p,c}$ = 87 ± 8.2 μA, $E^{\circ\prime}$ = −0.24 ± 0.01 V, and ΔE_p = 0.31 ± 0.02 V. These values are similar to those in CVs 3–5 in Fig. 2a. Note that each CV shown in Fig. 2 takes ~56 s to complete, and therefore we conclude that most of the sugar layer deposited onto the WE (Fig. 2a) dissolves in ~2 min.

We next examined the effect of sugar on the GE reaction using the MB–AgNP conjugate. Two different experiments were carried out using this conjugate, and in both cases Au was electrodeposited onto the carbon WE prior to analysis. In the first set of control experiments, the effect of sugar dried onto the WE was determined. These experiments were carried out in a similar fashion to those discussed above; specifically, the same protocol was used for drying sugar onto the WE.

Following preparation of the sugar layer, detection by GE/ASV was carried out as follows. First, the MB–AgNP conjugate suspension (Table 1 and Fig. S6:† sample-1) was pipetted only onto the WE as a 50.0 μL droplet. After a few seconds, the MB–AgNP conjugates concentrated on the WE electrode *via* the magnetic force. Second, the droplet on the WE was removed using a pipette, and then it was redispersed to cover the complete electrode assembly (*i.e.*, the WE, RE, and CQRE) of the *no*Flow device (Fig. S3b†). In this last step, care was taken to minimize disrupting the layer of MB–AgNP conjugates on the WE. An identical control experiment was also carried out in the absence of sugar.

The Ag ASVs in Fig. 3 are typical results for the foregoing experiments: the black ASV was obtained in the presence of predeposited sugar and the red Ag ASV was obtained in its absence. Qualitatively, the two ASVs appear similar, and even quantitatively the total GE/ASV charges are the same: 12.5 ± 0.4 μC in the presence of sugar and 12.6 ± 1.1 μC in its absence (based on five independent experiments). This finding indicates that the electrochemical processes that occur during the GE reaction are not significantly affected by sugar predeposited onto the WE. The results are also consistent with the CVs in Fig. 2, which indicated that the sugar layers dissolve within 120–180 s (the entire GE/ASV detection protocol takes 162 s).

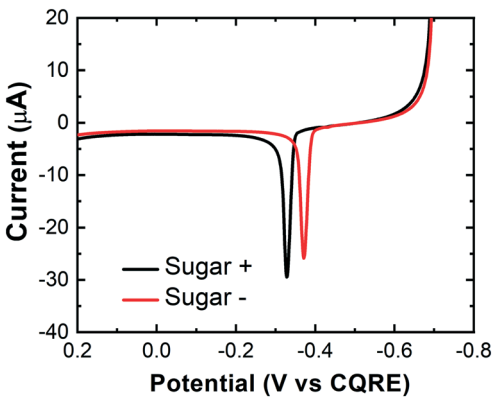

Fig. 3 ASVs for the detection of the MB–AgNP conjugate in absence (sugar –) and presence (sugar +) of sugar predried onto the *no*Flow WE. MB–AgNP conjugate: sample-0 and sample-1 (Table 1 and Fig. S6†); electrolyte: BCl; scan rate: 0.050 V s^{-1}; T = ~25 °C.

A second set of experiments was performed to determine the effect of sugar present in the electrolyte medium during electrochemical detection of Ag, but in this case sugar was not dried onto the WE. Specifically, the MB–AgNP conjugate, suspended in a sugar-containing matrix (Table 1 and Fig. S6:† sample-2) was pipetted onto the *no*Flow device as a 50.0 μL droplet covering the entire electrode assembly. The AgNPs were then detected by GE/ASV. For comparison, similar experiments were carried out in the absence of sugar (Table 1 and Fig. S6:† sample-0). The results, presented in Fig. S9,† indicated that the presence of sugar in the electrolyte solution has no detectable effect on the charge resulting from GE/ASV.

The results described in this section indicate that the mixture of sucrose and trehalose used in experiments to be described later has no significant impact on the GE/ASV detection processes as judged by the amount of charge collected during the final Ag oxidation step. Finally, we note that sucrose and trehalose are non-reducing disaccharides,[45] and they do not display any oxidation current in the potential window of the Ag ASV peak.

Analysis of preformed MB–AgNP conjugates at a single AgNP : MB ratio using the *hy*Flow device

In this section we discuss prototype assays carried out at the single AgNP : MB ratio of 441 AgNPs per MB (results from assays in which this ratio is varied will be discussed in a subsequent section). As discussed earlier in the context of Scheme 2, two types of assays were examined in the *hy*Flow system using preformed MB–AgNP conjugates: the 'wet' assay and the 'dry' assay. In the 'wet' assay, a suspension of the preformed MB–AgNP conjugate is injected into the inlet of the device (upstream of the electrochemical sensing area, Scheme 1b), transported to the electrochemical detection zone, and then concentrated at the WE by a magnetic force prior to GE/ASV detection. In contrast, the 'dry' assay is carried out by drying the MB–AgNP conjugate onto the paper electrode strip (Scheme 2, red box), and subsequently resolvating and concentrating it at the WE by a magnetic force prior to GE/ASV. The 'wet' assay was performed to obtain the maximum Ag charge that can be recovered from a sample suspension of the preformed MB–AgNP conjugate, and the 'dry' assay was designed to compare that value to the Ag charge recovered after the MB–AgNP conjugate was predried onto sample flow path and subsequently rehydrated.

In the 'wet' assay (Scheme 2), a suspension of MB–AgNP conjugate was analyzed by sequentially pipetting the following solutions into the inlet of the *hy*Flow device: 100.0 μL of DI water, 50.0 μL of an MB–AgNP conjugate sample, and then two 100.0 μL rinsing volumes of BCl solution (Movie S1†). When the final rinse solution ceased to flow through the channel, the GE/ASV electrochemical analysis was performed.

The first set of 'wet' assay experiments was carried out using 50.0 μL of MB–AgNP conjugate samples containing the range of wt% sugar indicated in Table 1 and Fig. S6† (sample set-3). The results of this experiment are shown as orange bars in Fig. 4, and they show the charge due to Ag oxidation is, within error, independent of the wt% sugar present in the solution. This result further confirms that sugar, present in the electrolyte solution, does not adversely impact analysis by GE/ASV.

The foregoing results were next compared to the 'dry' assay. In this case, 2.0 μL of the AgNP–MB conjugate suspension was directly drop-cast onto the yellow wax channel of the *hy*Flow paper electrode (Scheme 1a) 1.5 cm upstream from the center of the WE electrode (Table 1 and Fig. S6:† sample set-4) and allowed to dry overnight at ~25 °C in air. The device was then assembled and 100.0 μL of DI water was pipetted into the inlet. This solution was left in contact with the channel for 1.0 min to hydrate and resolvate the dried MB–AgNP conjugates (Movie S2†). Finally, the channel was rinsed with two 100.0 μL aliquots of BCl solution, and then the GE/ASV analysis was performed. Note that additional rinsing steps did not improve device performance.

The results of this experiment, shown in Fig. 4 as red bars, clearly underscore the importance of the co-deposited sugar for resolvation of the MB–AgNP conjugate in the 'dry' assay. Specifically, no GE/ASV charge is detected for 0 or 2 wt% sugar, while small but increasing signals are observed at the higher percentages. At 20 wt% sugar, the Ag charge detected is 6.3 ± 0.6 μC, which is well above the method detection limit of 0.04 μC. Accordingly, we carried out the remaining experiments involving dried assay components using 20 wt% sugar. Finally, Fig. S10† provides photos of the *hy*Flow electrodes obtained after the 'dry' assay experiments. These indicate the final locations of the MB–AgNP conjugates.

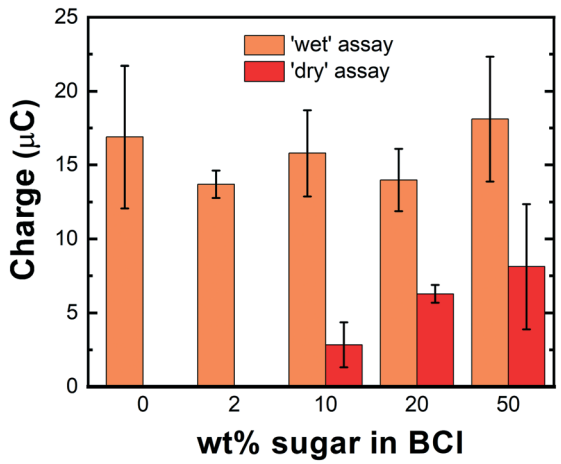

Fig. 4 Histogram showing the GE/ASV charge determined for detection of the MB–AgNP conjugates using the 'wet' and 'dry' assays. The MB–AgNP conjugate samples were prepared as indicated in Fig. S6† (sample set-3 and set-4). The error bars represent the standard deviations of three measurements for the 'wet' assay and five measurements for the 'dry' assay, obtained using independently fabricated paper electrodes.

We also investigated the effect of magnetic bead sizes on the GE/ASV signal using beads having diameters of 227 nm, 1.0 μm, and 2.8 μm. Normalized GE/ASV charges (based on the binding capacity of the beads) indicate that micron-scale MBs generate significantly higher signals compared to magnetic nanoparticles (see ESI† Fig. S11 for complete details). Accordingly, and unless otherwise indicated, the MB–AgNP conjugates used in subsequent experiments were prepared using 1.0 μm-diameter MBs.

Analysis of preformed MB–AgNP conjugates at multiple AgNP : MB ratios using the *hy*Flow device

Up to this point, all GE/ASV experiments were carried out using a single AgNP : MB ratio 441 (Table 1). In a real sandwich-type metalloimmunoassay, however, the target is present at varying concentrations and therefore the MBs will have different average AgNP coverages. Accordingly, we constructed a dose–response curve for both the 'wet' and 'dry' assays using different AgNP : MB ratios. These experiments were carried out in a similar manner to those previously described using BClS(20%) (BCl plus 20 wt% sugar) and using the *hy*Flow device.

The samples used for these 'wet' assay experiments are provided in Table 1 and Fig. S6† as sample set-5. These conjugates were prepared by mixing different concentrations of AgNP-bDNA solutions with a fixed volume of 1.0 μm-diameter MBs (see Table S1† for more details). Fig. 5a shows representative ASVs for the different AgNP : MB ratios in terms of the total AgNP concentrations. These voltammograms indicate that the Ag ASV current increases as a function of the concentration of the AgNPs in the sample. As shown in the inset of Fig. 5a, an AgNP concentration of 12 pM (average of 22 AgNPs per MB, Table S1†) can be differentiated from the baseline current. The average GE/ASV charge for six independent experiments per AgNP concentration are plotted in Fig. 5b. These data demonstrate that the GE/ASV charge increases linearly from 12 to 498 pM AgNPs, which corresponds to AgNP : MB ratios of 22 to 882, respectively. Note that when the AgNP concentration was increased to 996 pM (data not shown), the GE/ASV charge increased to only 26 ± 3.4 μC indicating saturation of the dose–response curve at concentrations somewhat lower than 498 pM. However, the *hy*Flow device has generated the highest Ag charge detected for a MB–AgNP conjugate using a hollow-channel, paper-based analytical device (Table S2†).

The foregoing results were next compared to the 'dry' assay. This set of experiments was carried out as discussed in

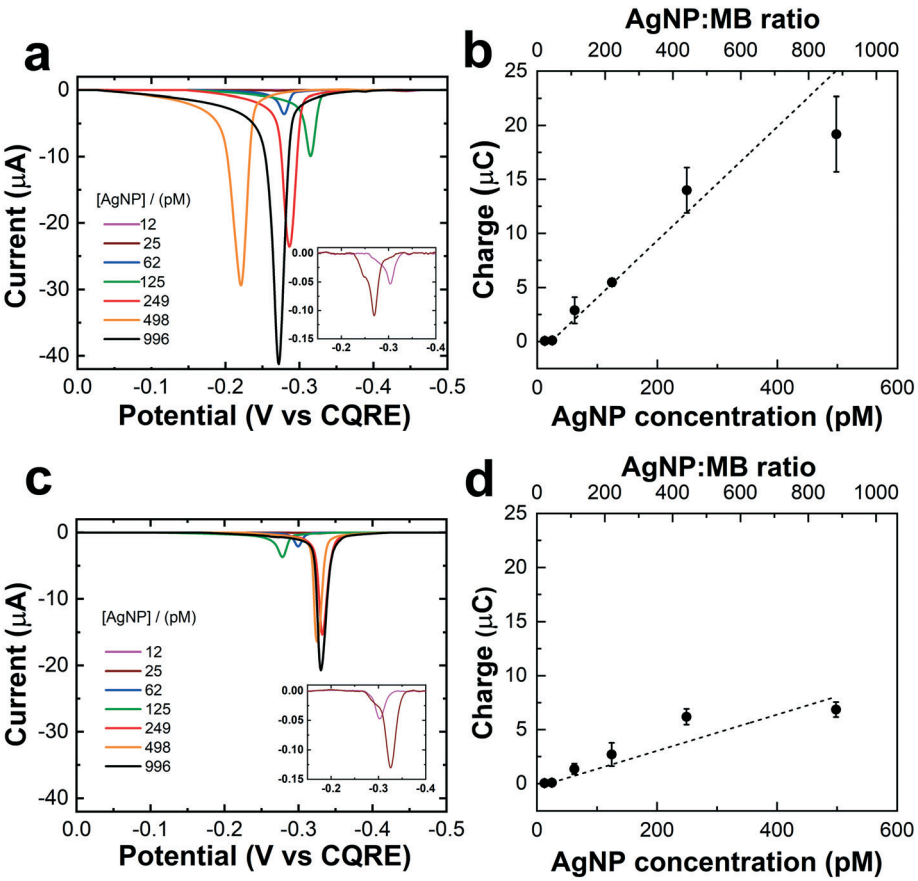

Fig. 5 Electrochemical results obtained using the *hy*Flow device for GE/ASV detection of MB–AgNP conjugates. (a) Baseline-corrected ASVs for detection of MB–AgNP conjugates using the 'wet' assay. The inset shows ASVs for the two lowest concentrations. The legend represents the concentration of AgNPs in the 50.0 μL of conjugate sample inserted into the *hy*Flow device. (b) Dose–response curve corresponding to the ASVs in (a). Note that the highest concentration (996 pM) shown in (a) is outside the linear range of the dose–response curve and therefore not plotted in (b). The error bars represent the standard deviations of six measurements obtained using independently fabricated paper electrodes. (c) Baseline-corrected ASVs for detection of MB–AgNP conjugates using the 'dry' assay. The inset shows ASVs for the two lowest concentrations. The legend represents the concentration of AgNPs in the resolvated conjugate sample. (d) Dose–response curve corresponding to the ASVs in (c). Note that the highest concentration (996 pM) shown in (c) is outside the linear range of the dose–response curve and therefore not plotted in (d). The error bars represent the standard deviations of six measurements obtained using independently fabricated paper electrodes. For all experiments the electrolyte solution was BCl, the scan rate was 0.050 V s^{-1}, the scan range was −0.70 V to 0.20 V, and T = ~25 °C. For (b) and (d), the dashed lines are the best linear fits to the data. For (a) and (c), the Ag oxidation peaks occur at different potentials due to the use of a carbon QRE.

the previous section. Here, the MB–AgNP conjugates were the same as those used for the experiments described in the previous paragraph (Table 1 and Fig. S6:† sample set-6). Fig. 5c shows representative ASVs for different AgNP concentrations for the 'dry' assay. These voltammograms indicate the same trend noted earlier: an increasing concentration of AgNPs leads to a higher ASV current. The average Ag charge measured for six independent experiments per AgNP concentration are plotted in Fig. 5d.

Interestingly, both the 'dry' and 'wet' assays yield a limit of detection of 12 pM AgNPs, and the two assays have about the same linear detection range. The sensitivity (slope of the calibration curve) is 0.053 μA pM^{-1} for the 'wet' assay and 0.017 μA pM^{-1} for the 'dry' assay. This means the sensitivity of the 'wet' assay is about three-fold higher than the 'dry' assay, which might be a consequence of some or all of the following reasons. First, some of the MB–AgNP conjugates might aggregate during the drying process and not resolvate correctly in the flow channel. Second, some conjugates could be nonspecifically adsorbed on the flow channel and hence not reach the WE. Third, different flow dynamics could lead to more or less favorable distribution patterns of the wet *vs.* pre-dried conjugates on the WE.

We investigated these hypotheses by performing a few control experiments as discussed in ESI† (Fig. S12 and S13). The results showed that the manner in which the MB–AgNP conjugates are distributed on the WE significantly impacts the final GE/ASV signal. Specifically, in the 'wet' assay, the conjugates were distributed uniformly on the WE, but in the 'dry' assay they tended to localize onto the side of the WE nearest the flow channel (Fig. S14†). We believe this unfavorable distribution adversely affects mass transfer of Au^{3+} and Ag^{+} during the GE reaction.

On-chip formation and detection of MB–AgNP conjugates

In a typical lateral flow sandwich immunoassay, an analyte forms a sandwich complex during capillary flow through the paper substrate.[7] This is achieved by drying the assay reagents on the paper substrate and then resolvating them during the analysis. Therefore, one crucial aspect of the operation of a lateral flow device is that the immunoassay forms within the device over a relatively short time interval. Accordingly, we investigated *in situ* formation of the MB–AgNP conjugate within the *hy*Flow device.

We examined two different on-chip assay formation protocols, which are referred to as 'instant mix-1' and 'instant mix-2'. For the 'instant mix-1' assay (Scheme 2), 2.0 μL of MBs (~7–10 × 10^9 MB per mL) in the BClS(20%) solution were drop-cast onto the yellow wax channel of the paper electrode, just as previously discussed for the 'dry' assay. Next, the MB–AgNP conjugate was formed on-chip by injecting 100.0 μL of a AgNP-bDNA/DI water solution (~6.0 × 10^{11} AgNPs per mL) into the chip to hydrate the dried MBs. This was followed by a 2 min incubation step, two washing steps (each using 100.0 μL of BCl solution), and finally GE/ASV detection. An identical control experiment was performed in the absence of MBs.

As shown in Fig. 6, this assay resulted in 7.3 ± 1.9 μC of GE/ASV charge for four independently prepared electrodes. A comparable GE/ASV signal was observed when the pre-dried volume of MBs was doubled (Fig. S15†). In contrast, the relevant control experiment (AgNP-bDNA control-1 in Fig. 6) exhibited negligible Ag charge. We conclude that the conjugate is able to form within the flow channel and be efficiently detected at the electrode assembly by GE/ASV.

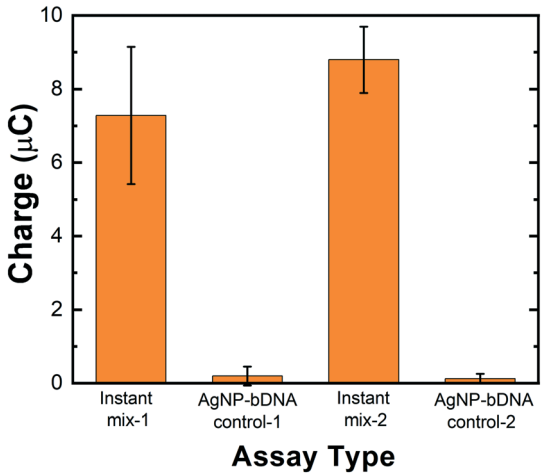

Fig. 6 Histogram showing the GE/ASV charge determined for the detection of MB–AgNP conjugates using the 'instant mix-1' and 'instant mix-2' assays. Identical control assays performed in the absence of MBs are labeled as 'AgNP-bDNA control-1' and 'AgNP-bDNA control-2'. The error bars represent the standard deviations of four measurements for the 'instant mix' assays and three measurements for the controls, all obtained using independently fabricated paper electrodes.

For the 'instant mix-2' assay, both AgNP-bDNA and MBs were drop-cast onto the flow channel of the *hy*Flow paper electrode. Specifically, 2.0 μL (~7–10 × 10^9 MB per mL) of MBs in the BClS(20%) solution was drop-cast onto the yellow wax channel of the paper electrode 1.5 cm upstream of the WE. Additionally, three 2.0 μL aliquots of AgNP-bDNA in BClS(20%) solution (~2.4 × 10^{13} AgNPs per mL) were also drop-cast in the flow channel in three separate zones. As shown in the lower-right illustration in Scheme 2, two of these aliquots were deposited upstream of the MBs and one was deposited downstream. The drop-cast reagents were then allowed to dry at ~25 °C overnight in the lab ambient.

The MB–AgNP conjugate was formed on-chip by injecting 100.0 μL of DI water into the inlet of the *hy*Flow device. The water facilitates hydration, resolvation, and passive mixing of the MBs with AgNP-bDNA (Movie S3†). Following a 2 min incubation in water and two subsequent washing steps (each using 100.0 μL of BCl solution), the Ag charge was determined by GE/ASV. As shown in Fig. 6, four independently conducted 'instant mix-2' assays yielded a GE/ASV charge of 8.8 ± 0.9 μC. A control experiment was also carried out in which pre-dried MBs were omitted, and as shown in Fig. 6 (AgNP-bDNA control-2) the resulting charge was negligible. On the basis of these results, we conclude that the assay forms even when both assay reagents are pre-dried within the flow channel of the *hy*Flow device.

Summary and conclusions

In summary, we have investigated an application of a hybrid paper/3D-printed microfluidic device (*hy*Flow) for electrochemical detection of a MB–AgNP model conjugate. This device was constructed to overcome problems associated with the use of MBs in paper-only analytical devices.[31,32,38]

There are three important conclusions arising from this study. First, the hollow channel within the *hy*Flow device facilitates transport of micron-scale MBs and minimizes nonspecific adsorption. Second, a 20 wt% mixture of sucrose and trehalose is effective for storing dried reagents within the channel of the *hy*Flow device. Moreover, the presence of sugar has no significant impact on the GE/ASV detection processes. Third, this hybrid device is capable of detecting a MB–AgNP conjugate in both pre-formed (off-chip) and *in situ* formed (on-chip) formats. We are presently investigating the applicability of the *hy*Flow device to detect a heart-failure biomarker, and the results of those experiments will be reported in due course.

Conflicts of interest

There are no conflicts to declare.

Acknowledgements

Research reported in this publication was supported by the National Heart, Lung, and Blood Institute of the National Institutes of Health under Award R01HL137601. The content

is solely the responsibility of the authors and does not necessarily represent the official views of the National Institutes of Health. We also thank the Robert A. Welch Foundation (Grant F-0032) for sustained support of our research. We gratefully acknowledge Dr. Livia Eberlin and Mr. Michael Keating for their assistance with the 3D printer. We thank Dr. Charlie Rabin and Ms. Nicole Pollok for helpful discussions.

References

1 W. Lu, K. Wang, K. Xiao, W. Qin, Y. Hou, H. Xu, X. Yan, Y. Chen, D. Cui and J. He, *Sci. Rep.*, 2017, **7**, 42414–42414.
2 Y. Wang, H. Xu, M. Wei, H. Gu, Q. Xu and W. Zhu, *IEEE J Transl Eng Health Med*, 2009, **29**, 714–718.
3 P. Yager, G. J. Domingo and J. Gerdes, *Annu. Rev. Biomed. Eng.*, 2008, **10**, 107–144.
4 S. A. Boppart and R. Richards-Kortum, *Sci. Transl. Med.*, 2014, **6**, 253rv252.
5 S. Nayak, N. R. Blumenfeld, T. Laksanasopin and S. K. Sia, *Anal. Chem.*, 2017, **89**, 102–123.
6 G. A. Posthuma-Trumpie, J. Korf and A. van Amerongen, *Anal. Bioanal. Chem.*, 2009, **393**, 569–582.
7 K. M. Koczula and A. Gallotta, *Essays Biochem.*, 2016, **60**, 111–120.
8 S. A. Butler, S. A. Khanlian and L. A. Cole, *Clin. Chem.*, 2001, **47**, 2131–2136.
9 A. W. Martinez, S. T. Phillips, M. J. Butte and G. M. Whitesides, *Angew. Chem., Int. Ed.*, 2007, **46**, 1318–1320.
10 A. W. Martinez, S. T. Phillips and G. M. Whitesides, *Proc. Natl. Acad. Sci. U. S. A.*, 2008, **105**, 19606–19611.
11 D. M. Cate, J. A. Adkins, J. Mettakoonpitak and C. S. Henry, *Anal. Chem.*, 2015, **87**, 19–41.
12 K. Yamada, T. G. Henares, K. Suzuki and D. Citterio, *Angew. Chem., Int. Ed.*, 2015, **54**, 5294–5310.
13 J. C. Cunningham, P. R. DeGregory and R. M. Crooks, *Annu. Rev. Anal. Chem.*, 2016, **9**, 183–202.
14 Y. Yang, E. Noviana, M. P. Nguyen, B. J. Geiss, D. S. Dandy and C. S. Henry, *Anal. Chem.*, 2017, **89**, 71–91.
15 H. Liu and R. M. Crooks, *J. Am. Chem. Soc.*, 2011, **133**, 17564–17566.
16 H. Liu, Y. Xiang, Y. Lu and R. M. Crooks, *Angew. Chem., Int. Ed.*, 2012, **51**, 6925–6928.
17 J. C. Cunningham, N. J. Brenes and R. M. Crooks, *Anal. Chem.*, 2014, **86**, 6166–6170.
18 J. C. Cunningham, K. Scida, M. R. Kogan, B. Wang, A. D. Ellington and R. M. Crooks, *Lab Chip*, 2015, **15**, 3707–3715.
19 X. Li, K. Scida and R. M. Crooks, *Anal. Chem.*, 2015, **87**, 9009.
20 S. E. Fosdick, M. J. Anderson, C. Renault, P. R. DeGregory, J. A. Loussaert and R. M. Crooks, *Anal. Chem.*, 2014, **86**, 3659–3666.
21 C. Renault, M. J. Anderson and R. M. Crooks, *J. Am. Chem. Soc.*, 2014, **136**, 4616–4623.
22 C. Renault, J. Koehne, A. J. Ricco and R. M. Crooks, *Langmuir*, 2014, **30**, 7030–7036.
23 J. Mettakoonpitak, K. Boehle, S. Nantaphol, P. Teengam, J. A. Adkins, M. Srisa-Art and C. S. Henry, *Electroanalysis*, 2016, **28**, 1420–1436.
24 W. Dungchai, O. Chailapakul and C. S. Henry, *Anal. Chem.*, 2009, **81**, 5821–5826.
25 P. D. Sinawang, V. Rai, R. E. Ionescu and R. S. Marks, *Biosens. Bioelectron.*, 2016, **77**, 400–408.
26 P. D. Sinawang, L. Fajs, K. Elouarzaki, J. Nugraha and R. S. Marks, *Sens. Actuators, B*, 2018, **259**, 354–363.
27 E. Dempsey and D. Rathod, *IEEE Sens. J.*, 2018, **18**, 1828–1834.
28 M. R. Akanda, H.-A. Joung, V. Tamilavan, S. Park, S. Kim, M. H. Hyun, M.-G. Kim and H. Yang, *Analyst*, 2014, **139**, 1420–1425.
29 D. Du, J. Wang, L. Wang, D. Lu and Y. Lin, *Anal. Chem.*, 2012, **84**, 1380–1385.
30 G. Ruiz-Vega, M. Kitsara, M. A. Pellitero, E. Baldrich and F. J. del Campo, *ChemElectroChem*, 2017, **4**, 880–889.
31 K. Scida, J. C. Cunningham, C. Renault, I. Richards and R. M. Crooks, *Anal. Chem.*, 2014, **86**, 6501–6507.
32 J. C. Cunningham, M. R. Kogan, Y.-J. Tsai, L. Luo, I. Richards and R. M. Crooks, *ACS Sens.*, 2016, **1**, 40–47.
33 P. R. Degregory, J. Tapia, T. Wong, J. Villa, I. Richards and R. M. Crooks, *J. Transl. Eng. Health Med.*, 2017, **5**, 1–6.
34 M. R. Kogan, N. E. Pollok and R. M. Crooks, *Langmuir*, 2018, **34**, 15719–15726.
35 D.-B. Wang, B. Tian, Z.-P. Zhang, J.-Y. Deng, Z.-Q. Cui, R.-F. Yang, X.-Y. Wang, H.-P. Wei and X.-E. Zhang, *Biosens. Bioelectron.*, 2013, **42**, 661–667.
36 J. Wu, M. Dong, C. Zhang, Y. Wang, M. Xie and Y. Chen, *Sensors*, 2017, **17**, 1286.
37 R. B. Channon, M. P. Nguyen, A. G. Scorzelli, E. M. Henry, J. Volckens, D. S. Dandy and C. S. Henry, *Lab Chip*, 2018, **18**, 793–802.
38 P. R. DeGregory, Y.-J. Tsai, K. Scida, I. Richards and R. M. Crooks, *Analyst*, 2016, **141**, 1734–1744.
39 X. Zhang, M. R. Servos and J. Liu, *J. Am. Chem. Soc.*, 2012, **134**, 7266–7269.
40 A. J. Bard, L. R. Faulkner, J. Leddy and C. G. Zoski, *Electrochemical methods: fundamentals and applications*, Wiley, New York, 2nd edn, 2001.
41 B. Wang, S. Tchessalov, M. T. Cicerone, N. W. Warne and M. J. Pikal, *J. Pharm. Sci.*, 2009, **98**, 3145–3166.
42 L. Chang, D. Shepherd, J. Sun, D. Ouellette, K. L. Grant, X. Tang and M. J. Pikal, *J. Pharm. Sci.*, 2005, **94**, 1427–1444.
43 C.-A. Chen, W.-S. Yeh, T.-T. Tsai, Y.-D. Li and C.-F. Chen, *Lab Chip*, 2019, **19**, 598–607.
44 H. Shekarchizadeh, A. A. Ensafi and M. Kadivar, *Mater. Sci. Eng. Carbon*, 2013, **33**, 3553–3561.
45 D. L. Nelson, A. L. Lehninger and M. M. Cox, *Lehninger principles of biochemistry*, Macmillan, 2008.